Distributed Control of the Attitude and Shape of a Flexible Spacecraft

Curtis A. Merrill* and Derek A. Paley†
University of Maryland, College Park, Maryland, 20742

The attitude and shape control of a large flexible spacecraft modeled as the hinged connection of multiple rigid bodies is considered. The spacecraft consists of a hub actuated by a reaction wheel and several appendages actuated by torque rods. The hinges rotate only in one direction, so a planar model is used. The appendages are connected by stiff springs and a dynamic model of the internal forces and moments of the system utilizes coordinates in the reference frame of the hub. Lyapunov analysis is performed to generate a distributed feedback control law for the reaction wheel and torque rods. Numerical simulations illustrate the performance of the proposed controller for orbital motion.

Nomenclature

m_i	=	mass of ith appendage
m_C	=	mass of hub
I_i	=	moment of inertia of ith appendage
I_C	=	moment of inertia of hub
L_i	=	length of ith appendage
s	=	length of hub
k_s	=	translational spring coefficient
c_s	=	translational damping coefficient
k_s	=	torsional spring coefficient
c_s	=	torsional damping coefficient
$\mathcal{I}$	=	Earth-centered inertial reference frame
$\mathcal{P}$	=	rotating reference frame centered on Earth
$\mathcal{A}$	=	body frame of spacecraft hub
$\mathcal{B}^{(i)}$	=	body frame of ith appendage
θ	=	colatitude of spacecraft
γ	=	hub attitude angle relative to inertial frame
α_i	=	appendage i attitude angle relative to hub

I. Introduction

Advances in technology have increased the feasibility and number of applications of large spacecraft. For instance, spacecraft with solar sails, large antennas, large solar arrays to meet high energy needs, extended truss structures, and manipulator arms have been proposed. One of the challenges of having large spacecraft is that the appendages to the spacecraft, due to weight constraints, may be flexible. Introducing flexibility creates a number of challenges to modeling and controlling the spacecraft.

One of the primary challenges in controlling a large, flexible spacecraft is dealing with the vibrations in the flexible appendages that are excited by attitude maneuvers performed by the hub. These oscillations can significantly affect the attitude control of a spacecraft by reducing stability and increasing the settling time. Additionally, structural vibrations can pose problems if maintaining flatness of the appendage is important for performance, or if they reduce the lifespan of the structure. Without aerodynamic drag, there is little to no environmental damping and, with mass being a primary

*Graduate student, Department of Aerospace Engineering, University of Maryland, College Park, MD, 20742
†Willis H. Young Jr. Professor of Aerospace Engineering Education, Department of Aerospace Engineering and Institute for Systems Research, University of Maryland, College Park, MD 20742. AIAA Senior Member

concern of spacecraft structures, it becomes difficult to solve this problem by stiffening the appendages or connections. One way of addressing this problem has been through investigating spatially distributed actuation and control to regulate the attitude and shape of the entire structure.

One method that has been investigated for mitigating structural oscillation is by developing attitude control laws that minimize excitation. A super-twisting sliding mode control is developed in [1] to simultaneously perform attitude tracking and vibration suppression. An extended disturbance observer and backstepping controller is proposed in [2] for attitude stabilization by rejecting disturbances resulting from the flexible spacecraft. In [3], the flexible appendages are modeled using partial differential equations and distributed and boundary controllers are implemented to compensate for and suppress the disturbances and vibrations of the structure. [4] treats the oscillations as a disturbance, and derives a compensator and controller to guarantee robust attitude control. A controller that plans constrained low-jerk maneuvers is provided in [5].

Another research area involves active vibration suppression using additional actuators. The use of piezoelectric actuators on flexible structures to perform active vibration suppression has been studied. In [6], a constrained torque distribution algorithm along with a shape input controller for piezoelectric actuators are used for attitude and shape control. A robust control scheme based on a distributed observer and controller framework is developed in [7], which also uses piezoelectric actuation for flatness control of flexible appendages. However, due to size-at-launch constraints, spacecraft with a large area-to-bus size ratio must be folded and then deployed after launch. Research in deployable space structures, such as [8], studies the deployment dynamics of folded spacecraft structures. Whereas the flexing in large lightweight spacecraft structures occurs in the structure itself, the flexing in a multibody deployable space structure may be more significant at the hinges. Consequently, while piezoelectric actuators may suppress vibrations in a flexible appendage, their utility is limited if the main source of flexibility of a spacecraft is in the interface between bodies, which might occur in a deployable space structure. To better address shape control of a multibody flexible spacecraft, instead of actuating the shape of an appendage, [9] assumes that actuators are mounted on the interface between an appendage and the hub, and a control law is proposed to provide attitude and shape control. In [10] a model is formed and a control law proposed where control moment gyros are distributed across the flexible structure to provide vibration suppression. This work is extended in [11], where a global matrix formulation of the dynamics is proposed for a flexible multibodied spacecraft.

In the case where the number of appendages is large or where the area-to-bus size ratio is large, the added mass for each additional actuator could prohibit implementation. With piezoelectric actuators being ineffective at controlling appendage interface flexibility and with reaction wheels and hinges being potentially too massive, there is a need to control large flexible multibody spacecraft using actuation that is better suited for the requirements of the spacecraft mission. In this paper, a multibody spacecraft consisting of a hub and an arbitrary number of appendages with flexible connections between each of the bodies is considered. The proposed actuation consists of a reaction wheel in the spacecraft hub and a magnetic torque rod in each of the appendages. A dynamic model for the hub and appendages is developed using coordinates relative to a body-frame attached to the hub. Lyapunov-based control design generates a stable feedback control law for the torque rods and reaction wheels.

The contributions of this paper are as follows: (1) a dynamic model of a spacecraft that is flexible in one direction expressed in the reference frame of the spacecraft hub; (2) a controller based on a Lyapunov design that tracks a desired attitude and suppresses oscillations in the appendages. Numerical simulations are performed to validate the efficacy of the proposed control law under idealized conditions and under more realistic conditions. Effective shape control would enable successful deployment of larger and lighter structures on spacecraft by mitigating the risk of structural oscillation.

The paper is organized as follows. The problem statement and the spacecraft concept are given in Section II. The dynamic model of the spacecraft is developed in Section III and the proposed controller is presented in Section IV. Simulation results are shown in Section V, and a conclusion is given in Section VI

II. Preliminaries

Consider a spacecraft that consists of a central hub with a set of appendages connected flexibly via damped spring hinges. The damped hinges could be thought to model a highly flexible structure or a large spacecraft that must be folded for launch and deployed in orbit, leading to a necessary lack of rigidity. Assume that the hinges have only one degree of freedom, thus the motion considered is restricted to the orbital plane. As a result, it is only necessary to consider two-dimensional dynamics.

Render.PNG 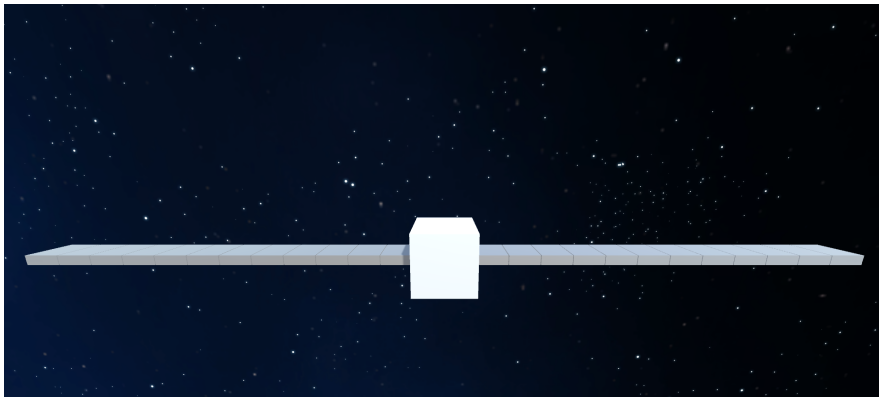

Fig. 1 Hub and appendage spacecraft structure concept art, depicting the hub and a series of appendages

For a spacecraft with a structure shown in Fig. 1, the indexing scheme shown in Fig. 2 is used to refer to each of the components of the spacecraft.

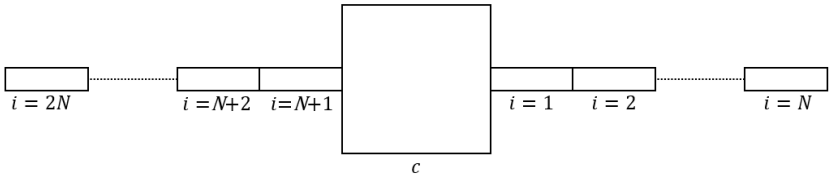

Fig. 2 Indexing of appendages for proposed spacecraft structure

Consider an Earth-centered inertial frame, $\mathcal{I} = (O, \hat{\mathbf{e}}_x, \hat{\mathbf{e}}_y, \hat{\mathbf{e}}_3)$, an Earth-centered rotating frame that rotates at the orbital rate of the spacecraft $\mathcal{P} = (O, \hat{\mathbf{e}}_r, \hat{\mathbf{e}}_\theta, \hat{\mathbf{e}}_3)$, a body-fixed frame affixed to the central hub of the spacecraft $\mathcal{A} = (C, \hat{\mathbf{a}}_1, \hat{\mathbf{a}}_2, \hat{\mathbf{a}}_3)$, and body-fixed frames affixed to each of the component appendages to the spacecraft $\mathcal{B}^{(i)} = (B^{(i)}, \hat{\mathbf{b}}_1^{(i)}, \hat{\mathbf{b}}_2^{(i)}, \hat{\mathbf{b}}_3^{(i)})$, $i = 1, ..., 2N$. Angle θ defines the relative orientation of $\mathcal{P}$ with respect to $\mathcal{I}$, γ is the orientation of $\mathcal{A}$ with respect to $\mathcal{I}$, and α_i is the orientation of $\mathcal{B}^{(i)}$ with respect to $\mathcal{A}$.

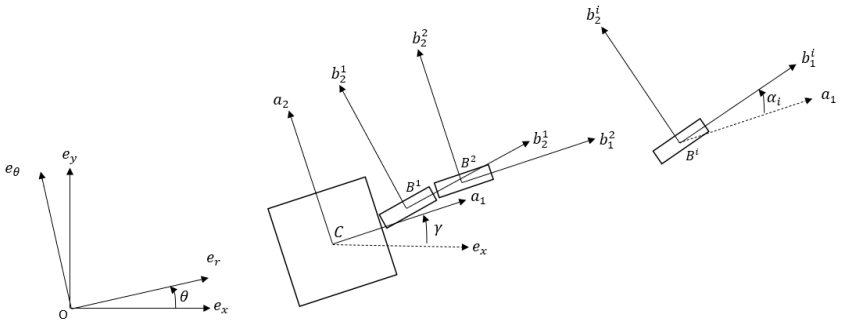

Fig. 3 Reference frames used for the flexible spacecraft model. Frame C is fixed to the hub; frames $B^{(i)}, i = 1, ..., 2N$, are fixed to each appendage

III. Spacecraft Dynamics

This section derives the dynamics of the spacecraft in the reference frame of the hub, and models its internal forces, control inputs, and disturbances to yield the equations of motion for the system.

A. Multi-body Dynamics

First, the dynamics of the hub C and each of the appendages are derived. For the hub,

$$\mathbf{r}_{C/O} = x_C\hat{\mathbf{e}}_x + y_C\hat{\mathbf{e}}_y \tag{1}$$

$$^{\mathcal{I}}\mathbf{v}_{C/O} = \dot{x}_C\hat{\mathbf{e}}_x + \dot{y}_C\hat{\mathbf{e}}_y \tag{2}$$

$$^{\mathcal{I}}\mathbf{a}_{C/O} = \ddot{x}_C\hat{\mathbf{e}}_x + \ddot{y}_C\hat{\mathbf{e}}_y. \tag{3}$$

Consider reference frame $\mathcal{A}$. The inertial derivative of unit vector $\hat{\mathbf{a}}_1$ is $^{\mathcal{I}}\frac{d}{dt}\hat{\mathbf{a}}_i = {}^{\mathcal{I}}\boldsymbol{\omega}^A \times \hat{\mathbf{a}}_i$, where $^{\mathcal{I}}\boldsymbol{\omega}^A = \dot{\gamma}\hat{\mathbf{a}}_3$ is the angular velocity of frame A in the inertial reference frame. Using the two-dimensional orbital plane reference frame, the angular velocity of the hub is restricted to the $\hat{\mathbf{a}}_3 = \hat{\mathbf{e}}_3$ direction, with magnitude $\dot{\gamma}$. For the appendages,

$$\mathbf{r}_{i/O} = \mathbf{r}_{C/O} + \mathbf{r}_{i/C} = x_C\hat{\mathbf{e}}_x + y_C\hat{\mathbf{e}}_y + x_{i/C}\hat{\mathbf{a}}_1 + y_{i/C}\hat{\mathbf{a}}_2 \tag{4}$$

Differentiating with respect to time yields

$$\begin{aligned}{}^{\mathcal{I}}\mathbf{v}_{i/O} = {}^{\mathcal{I}}\frac{d}{dt}\mathbf{r}_{i/O} &= \dot{x}_C\hat{\mathbf{e}}_x + \dot{y}_C\hat{\mathbf{e}}_y + \dot{x}_{i/C}\hat{\mathbf{a}}_1 + \dot{y}_{i/C}\hat{\mathbf{a}}_2 + x_{i/C}(\dot{\gamma}\hat{\mathbf{e}}_3 \times \hat{\mathbf{a}}_1) + y_{i/C}(\dot{\gamma}\hat{\mathbf{e}}_3 \times \hat{\mathbf{a}}_2) \\ &= \dot{x}_C\hat{\mathbf{e}}_x + \dot{y}_C\hat{\mathbf{e}}_y + \dot{x}_{i/C}\hat{\mathbf{a}}_1 + \dot{y}_{i/C}\hat{\mathbf{a}}_2 + \dot{\gamma}x_{i/C}\hat{\mathbf{a}}_2 - \dot{\gamma}y_{i/C}\hat{\mathbf{a}}_1\end{aligned}$$

Differentiating again yields the inertial acceleration, i.e.,

$${}^{\mathcal{I}}\mathbf{a}_{i/O} = \ddot{x}_C\hat{\mathbf{e}}_x + \ddot{y}_C\hat{\mathbf{e}}_y + \ddot{x}_{i/C}\hat{\mathbf{a}}_1 + \ddot{y}_{i/C}\hat{\mathbf{a}}_2 + \ddot{\gamma}x_{i/C}\hat{\mathbf{a}}_2 - \ddot{\gamma}y_i\hat{\mathbf{a}}_1 + 2\dot{\gamma}\dot{x}_{i/C}\hat{\mathbf{a}}_2 - 2\dot{\gamma}\dot{y}_{i/C}\hat{\mathbf{a}}_1 - \dot{\gamma}^2x_{i/C}\hat{\mathbf{a}}_1 - \dot{\gamma}^2y_{i/C}\hat{\mathbf{a}}_2 \tag{5}$$

Euler's first law is applied to the hub and to each appendage. It is convenient to express the forces on the hub in reference frame $\mathcal{A}$. The total force on the hub is defined as $\mathbf{F}_C = X_C\hat{\mathbf{a}}_1 + Y_C\hat{\mathbf{a}}_2$.

$$\ddot{x}_C\hat{\mathbf{a}}_1 + \ddot{y}_C\hat{\mathbf{a}}_2 = \frac{X_C}{m_C}\hat{\mathbf{a}}_1 + \frac{Y_C}{m_C}\hat{\mathbf{a}}_2 \tag{6}$$

The sum of the forces on each appendage is $\mathbf{F}_i = X_i\hat{\mathbf{a}}_1 + Y_i\hat{\mathbf{a}}_2$. Applying Euler's first law to the ith appendage yields

$${}^{\mathcal{I}}\mathbf{a}_{i/O} = \frac{X_i}{m_i}\hat{\mathbf{a}}_1 + \frac{Y_i}{m_i}\hat{\mathbf{a}}_2 \tag{7}$$

One of the primary goals is to control the shape of the entire spacecraft in order to keep it flat and aligned with the hub. Analyzing the dynamics of each appendage relative to the hub is convenient, because the resulting control problem is to drive the relative angle and relative translational and angular velocities to zero. To express the equations of motion in the hub's reference frame, the kinematics for the appendage and hub are substituted into 5 and the expression is rearranged to solve for the acceleration of the appendages relative to the hub, i.e.,

$$\ddot{x}_{i/C}\hat{\mathbf{a}}_1 + \ddot{y}_{i/C}\hat{\mathbf{a}}_2 = \frac{X_i}{m_i}\hat{\mathbf{a}}_1 + \frac{Y_i}{m_i}\hat{\mathbf{a}}_2 - \frac{X_C}{m_C}\hat{\mathbf{a}}_1 - \frac{Y_C}{m_C}\hat{\mathbf{a}}_2 - \ddot{\gamma}x_{i/C}\hat{\mathbf{a}}_2 + \ddot{\gamma}y_i\hat{\mathbf{a}}_1 - 2\dot{\gamma}\dot{x}_{i/C}\hat{\mathbf{a}}_2 + 2\dot{\gamma}\dot{y}_{i/C}\hat{\mathbf{a}}_1 + \dot{\gamma}^2x_{i/C}\hat{\mathbf{a}}_1 + \dot{\gamma}^2y_{i/C}\hat{\mathbf{a}}_2. \tag{8}$$

The terms are collected to arrive at the following scalar differential equations.

$$\ddot{x}_{i/C} = \frac{X_i}{m_i} - \frac{X_C}{m_C} + \ddot{\gamma}y_{i/C} + 2\dot{\gamma}\dot{y}_{i/C} + \dot{\gamma}^2x_{i/C} \tag{9}$$

$$\ddot{y}_{i/C} = \frac{Y_i}{m_i} - \frac{Y_C}{m_C} - \ddot{\gamma}x_{i/C} - 2\dot{\gamma}\dot{x}_{i/C} + \dot{\gamma}^2y_{i/C} \tag{10}$$

Next Euler's second law is applied to the hub and appendages, with the total internal moments on each defined as M_C and M_i respectively.

$$\frac{d}{dt}{}^{\mathcal{I}}\mathbf{h}_C = \frac{d}{dt}I_C\dot{\gamma}\hat{\mathbf{a}}_3 = I_C\ddot{\gamma}\hat{\mathbf{a}}_3 = M_C\hat{\mathbf{a}}_3 \tag{11}$$

$$\frac{d}{dt}{}^{\mathcal{I}}\mathbf{h}_i = \frac{d}{dt}I_p(\dot{\gamma} + \dot{\alpha}_i)\hat{\mathbf{a}}_3 = I_p(\ddot{\gamma} + \ddot{\alpha}_i)\hat{\mathbf{a}}_3 = M_i\hat{\mathbf{a}}_3 \tag{12}$$

The state for each appendage described in two dimensions is

$$\xi_i = \begin{bmatrix} x_{i/C} & y_{i/C} & \alpha_{i/C} & \dot{x}_{i/C} & \dot{y}_{i/C} & \dot{\alpha}_{i/C} \end{bmatrix}^T \tag{13}$$

The modeling of the forces and moments acting on each component, i.e., X_C, Y_C, M_C, X_i, Y_i, and M_i, are defined next.

B. Force Model

Assume that the appendages are connected to each other and two appendages are connected to the hub with damped hinges. The attachment force of each hinge is modeled as a spring with spring coefficient k_s and damping coefficient c_s. The attachment moment is modeled as a torsion spring that is linearly proportional to the relative angle between the components that it connects, with spring coefficient k_t and damping coefficient c_t. With the torsion spring model, the relative force between two components can be computed by determining the relative position and velocity of adjoining edges. The relative position and velocity of adjoining edges of the ith appendage to its adjacent appendages for $i = (1, ..., N)$ is expressed as

$$\mathbf{r}_{i,i+1} = \mathbf{r}_{i/C} + \frac{L_i}{2}\hat{\mathbf{b}}_1^{(i)} - \mathbf{r}_{i+1/C} + \frac{L_{i+1}}{2}\hat{\mathbf{b}}_1^{(i+1)} \tag{14}$$

$${}^{\mathcal{A}}\mathbf{v}_{i,i+1} = {}^{\mathcal{A}}\mathbf{v}_{i/C} + \frac{L_i}{2}\frac{{}^{\mathcal{A}}d}{dt}\hat{\mathbf{b}}_1^{(i)} - {}^{\mathcal{A}}\mathbf{v}_{i+1/C} + \frac{L_{i+1}}{2}\frac{{}^{\mathcal{A}}d}{dt}\hat{\mathbf{b}}_1^{(i+1)} \tag{15}$$

$$\mathbf{r}_{i,i-1} = \mathbf{r}_{i/C} - \frac{L_i}{2}\hat{\mathbf{b}}_1^{(i)} - \mathbf{r}_{i-1/C} - \frac{L_{i-1}}{2}\hat{\mathbf{b}}_1^{(i-1)} \tag{16}$$

$${}^{\mathcal{A}}\mathbf{v}_{i,i-1} = {}^{\mathcal{A}}\mathbf{v}_{i/C} - \frac{L_i}{2}\frac{{}^{\mathcal{A}}d}{dt}\hat{\mathbf{b}}_1^{(i)} - {}^{\mathcal{A}}\mathbf{v}_{i-1/C} - \frac{L_{i-1}}{2}\frac{{}^{\mathcal{A}}d}{dt}\hat{\mathbf{b}}_1^{(i-1)}. \tag{17}$$

For $i = (N+1, ..., 2N)$ the negation of the shown position and velocity is used due to the indexing scheme increasing in the opposite direction on the other side of the spacecraft. The resulting internal force on an appendage from an adjacent appendage can then be expressed as

$$\mathbf{F}_{i,j} = -k_s\mathbf{r}_{i,j} - c_s^{\mathcal{A}}\mathbf{v}_{i,j} \tag{18}$$

The torque resulting from the internal forces is

$$\mathbf{T}_{i,i+1} = \frac{L_i}{2}\hat{\mathbf{b}}_1^{(i)} \times \mathbf{F}_{i,i+1}, \quad \mathbf{T}_{i,i-1} = -\frac{L_i}{2}\hat{\mathbf{b}}_1^{(i)} \times \mathbf{F}_{i,i-1} \tag{19}$$

The internal moment resulting from the spring hinge is modeled as

$$\mathbf{M}_{i,i+1} = -k_t(\alpha_i - \alpha_{i+1}) - c_t(\dot{\alpha}_i - \dot{\alpha}_{i-1}), \quad \mathbf{M}_{i,i-1} = k_t(\alpha_i - \alpha_{i-1}) - c_t(\dot{\alpha}_i - \dot{\alpha}_{i-1}) \tag{20}$$

The forces and moments for the end appendages and for the hub are shown in the appendix in Section VII.A. These equations provide a complete description of the internal forces and moments acting on the proposed spacecraft. The unforced dynamics of the spacecraft can then be completely described as a state-space system. Due to the primary investigation being attitude and shape control, the translational dynamics of the central hub can be excluded from the system model, because the translational dynamics of the appendages are expressed in the reference frame of the hub. Therefore, the total state of the system $\boldsymbol{\eta}$ can be defined as

$$\boldsymbol{\eta} = \begin{bmatrix} \gamma & \dot{\gamma} & \xi_1^T & \xi_2^T & \dots & \xi_N^T & \xi_{N+1}^T & \dots & \xi_{2N}^T \end{bmatrix}^T, \tag{21}$$

and the unforced dynamics can be written as

$$\dot{\boldsymbol{\eta}} = \boldsymbol{f}(\boldsymbol{\eta}) \tag{22}$$

For convenience, the portion of the state for the hub orientation, γ and $\dot{\gamma}$ will be denoted $\boldsymbol{\eta}_C$ and the rest of the state vector describing all appendages will be denoted $\boldsymbol{\eta}_p$.

C. Control Inputs

Assume that there is a reaction wheel in the hub and that each of the appendages are equipped with a torque rod. The reaction wheel has some saturation limit K_{rw} and that the control input is simply the reaction wheel torque, so that the torque generated by the reaction wheel in response to control input u_{rw} is

$$\tau_{\text{rw}} = \text{sat}(u_{\text{rw}}) = \begin{cases} -K_{\text{rw}} & u_{\text{rw}} \le -K_{\text{rw}} \\ u_{\text{rw}} & -K_{\text{rw}} < u_{\text{rw}} < K_{\text{rw}} \\ K_{\text{rw}} & u_{\text{rw}} \ge K_{\text{rw}} \end{cases}.$$

Assume each torque rod is aligned with the $\mathbf{b}_1^{(i)}$ axis of the body frame assigned to the respective spacecraft segment. Torque rods typically operate by turning on and off electrical current through a coil, resulting in a discrete set of control inputs. Assume that the control input is modeled as the desired dipole generated by the torque rod, and the maximum magnitude of the dipole is denoted K_{tr}. To implement the discrete control input set, the sign function may be used. However, to avoid chatter that can occur around $u_{\text{tr}} = 0$, the deadband function is used instead. Then the possible inputs for each torque rod are as follows:

$$m_i = K_{\text{tr}}\text{dbd}(u_{\text{tr}}, \lambda) = \begin{cases} -K_{\text{tr}} & u_{\text{tr}} < -\lambda \\ 0 & -\lambda < u_{\text{tr}} < \lambda \\ K_{\text{tr}} & u_{\text{tr}} > \lambda \end{cases}$$

The magnetic dipole resulting from the torque rod expressed in the Earth-centered polar frame is

$$\mathbf{m}_i = \begin{bmatrix} m_i \cos\psi_i \\ m_i \sin\psi_i \\ 0 \end{bmatrix}, \tag{23}$$

where ψ is defined as the angle between the spacecraft's colatitude θ and the body frame axis $\hat{\mathbf{b}}_2^{(i)}$, i.e., $\psi_i = \theta - \gamma - \alpha_i$, for the appendages. The Earth's magnetic field is modeled as a dipole and in the fixed reference frame of the orbital plane can be expressed as

$$\mathbf{B} = \begin{bmatrix} 2H_e \left(\frac{R}{\rho}\right)^3 \cos\theta \\ H_e \left(\frac{R}{\rho}\right)^3 \sin\theta \\ 0 \end{bmatrix}. \tag{24}$$

The torque developed by this control input can then be computed by taking the cross-product of the resulting torque rod dipole 23 and the Earth's magnetic field 24, i.e.,

$$\boldsymbol{\tau}_{\text{tr}} = 2H_e \left(\frac{R}{\rho}\right)^3 m_i(\sin\psi_i \sin\theta - 2\cos\psi_i cos\theta)\hat{\mathbf{e}}_3 \tag{25}$$

D. Gravity Gradient Effects

When considering large spacecraft, one of the largest disturbance moments comes from the gravity gradient effect, which results from each part of the spacecraft experiencing slightly different magnitudes of gravitational force from Earth. The generalized first-order approximation of gravity gradient torque is [12]

$$\boldsymbol{\tau}_{GG} = \frac{3\mu}{\rho^5}\boldsymbol{\rho} \times [I]\boldsymbol{\rho}, \tag{26}$$

where $\boldsymbol{\rho} = \rho\hat{\mathbf{e}}_r$ is the vector from the center of the Earth to the center of mass of the body and $[I]$ is its moment of inertia. In the body frames of the hub and appendages, respectively,

$$\boldsymbol{\rho}_C = \rho_C \cos(\theta - \gamma)\hat{\mathbf{a}}_1 - \rho_C \sin(\theta - \gamma_)\hat{\mathbf{a}}_2, \quad \boldsymbol{\rho}_i = \rho_i \cos(\psi_i)\hat{\mathbf{b}}_1^{(i)} - \rho_i \sin(\psi_i)\hat{\mathbf{b}}_2^{(i)} \tag{27}$$

We approximate the moment of inertia tensor of the hub as a cube of side-length s and the appendages as thin rods of length L. The moment of inertia tensors are then as follows

$$I_C = \begin{bmatrix} \frac{1}{6}s^2 & 0 & 0 \\ 0 & \frac{1}{6}s^2 & 0 \\ 0 & 0 & \frac{1}{6}s^2 \end{bmatrix} \tag{28}$$

$$I_i = \begin{bmatrix} \frac{1}{12}L_i^2 & 0 & 0 \\ 0 & 0 & 0 \\ 0 & 0 & \frac{1}{12}L_i^2 \end{bmatrix} \tag{29}$$

The first-order approximation for gravity gradient torque for the hub is therefore zero and, for the appendages

$$\boldsymbol{\tau}_{GG} = -\frac{\mu m_i L_i^2}{8\rho^3}\sin(2\psi)\hat{\mathbf{a}}_3 \tag{30}$$

The gravity gradient effect is applied as a disturbance in numerical simulations to evaluate control robustness.

IV. Spacecraft Control

This section considers reference tracking of an attitude trajectory at a constant angular rate that represents orbital motion. In order to track the desired trajectory while maintaining spacecraft flatness, a suitable controller is designed.

A. State Feedback Control

The equilibrium of the system is when each appendage is flat and unmoving relative to the hub reference frame and in its desired position. The dynamics of the undisturbed system are linearized by taking the Jacobian of the dynamics at the equilibrium condition. By using the reference frame of the hub to express the dynamics, the orientation of the reference frame γ does not appear in the Jacobian of the unforced state dynamics. Specifically, the equilibrium for $x_{i/C}$ is $x_{\text{eq}}^{(i)} = \pm(\frac{s}{2} + \frac{2i-1}{2}L)$; it is positive for $i = 1, ..., N$ and negative for $i = N+1, ..., 2N$. The equilibrium state of each appendage is $\xi_{\text{eq}}^{(i)} = \pm\begin{bmatrix} x_{\text{eq}}^{(i)} & 0 & 0 & 0 & 0 & 0 \end{bmatrix}^T$. Because the dynamics of each component of the satellite are explicitly dependent on only the states of the adjacent components and the reference frame of the hub, the linearized state dynamics can be written in block matrix form, where the blocks are defined as

$$A_C = \frac{\partial \dot{\boldsymbol{\eta}}_C}{\partial \boldsymbol{\eta}}, \quad A_C^{(i)} = \frac{\partial \dot{\boldsymbol{\xi}}_i}{\partial \boldsymbol{\eta}_C}, \quad A_i = \frac{\partial \dot{\boldsymbol{\xi}}_i}{\partial \boldsymbol{\eta}_p}. \tag{31}$$

The total system Jacobian is

$$A = \frac{\partial \mathbf{f}}{\partial \boldsymbol{\eta}} = \begin{bmatrix} A_C & 0 & \dots & \dots & 0 \\ A_C^{(1)} & A_1 & 0 & \dots & 0 \\ A_C^{(2)} & 0 & A_2 & \dots & 0 \\ \vdots & \vdots & \vdots & \ddots & \vdots \\ A_C^{(2N)} & 0 & 0 & \dots & A_{2N} \end{bmatrix}. \tag{32}$$

To evaluate the stability of the unforced spacecraft structure, the eigenvalues of A are computed. For any number of appendages, A has two eigenvalues of 0 and the rest have a negative real part. The two imaginary axis eigenvalues correspond to the orientation and angular velocity of the hub, because in the unforced case there is no external damping of the hub's angular motion. Thus, the dynamics of the appendages are exponentially stable, but the dynamics of the hub are not.

The input vector is defined as

$$\mathbf{u} = \begin{bmatrix} u_1 & u_2 & \dots & u_{2N} & u_{\text{rw}} \end{bmatrix}^T. \tag{33}$$

The input-to-state linearization of the dynamics can similarly be described in block matrix form by taking

$$B_C = \frac{\partial \dot{\boldsymbol{\eta}}_C}{\partial \mathbf{u}} = \begin{bmatrix} 0 & \dots & 0 \\ 0 & \dots & \frac{1}{I_C} \end{bmatrix} \tag{34}$$

$$B_i = \frac{\partial \dot{\boldsymbol{\xi}}_i}{\partial \mathbf{u}} = \begin{bmatrix} 0^{4\times1} & \dots & \dots & \dots & \dots & \dots & \dots & 0^{4\times1} \\ 0 & \dots & \dots & \dots & \dots & \dots & 0 & -\frac{x_{\text{eq}}^{(i)}}{I_C} \\ 0 & \dots & 0 & \frac{E}{I_p} & 0 & \dots & 0 & -\frac{1}{I_C} \end{bmatrix}, \tag{35}$$

where $E = 2H_e(\frac{R}{\rho})^3$ and $\frac{E}{I_p}$ appears in the ith column of B_i. The total matrix can then be expressed as

$$B = \frac{\partial \boldsymbol{\eta}}{\partial \mathbf{u}} = \begin{bmatrix} B_C^T & B_1^T & B_2^T & \dots & B_{2N}^T \end{bmatrix}^T \tag{36}$$

and the portion of the matrix dealing with the torque rods can be expressed as

$$B_p = \begin{bmatrix} B_1^T & B_2^T & \dots & B_{2N}^T \end{bmatrix}^T \tag{37}$$

From the linearized equations $\dot{\boldsymbol{\eta}} = A\boldsymbol{\eta} + B\boldsymbol{u}$, a linear-quadratic regulator (LQR) can be applied to generate a gain matrix such that the state feedback control law $\boldsymbol{u} = -K\boldsymbol{\eta}$ is an optimal controller that drives the linearized set of differential equations to their equilibrium. LQR serves as a good baseline controller, because it is optimal, can be tuned to exhibit desired performance characteristics, and is computationally inexpensive. However, because the actuators are modeled with physical operation characteristics in mind, additional nonlinearities are introduced into the system. Specifically, the saturation nonlinearities and discrete control inputs from Section III.C must be applied to the output of the LQR controller before it is applied to the system. The addition of these nonlinearities undermines the optimality and performance of the LQR and motivates the Lyapunov-based based control design described next.

B. Lyapunov-based Control

Consider the following assumptions: each appendage is the same size, the hub is significantly larger and more massive than each individual appendage, the appendages do not reach very high angular rates relative to the hub, the relative translational velocities of the appendages remain small, and the reaction wheels produce torque on the order of milli-Newton meters, i.e.,

$$L_i = L_j \quad \forall i, j \in \{1, ..., 2N\} \tag{38}$$

$$I_p \ll I_C \tag{39}$$

$$\dot{\alpha}_i \ll 1 \tag{40}$$

$$\dot{x_{i/C}} = \dot{y_{i/C}} \approx 0 \tag{41}$$

$$u_{rw} \ll 1 \tag{42}$$

An energy-like function that describes the kinetic and potential energy of the spacecraft appendages in the reference frame of the hub is

$$T(\boldsymbol{\eta}_p) = \frac{1}{2} \sum_{i=1}^{2N} \left[m_i(\dot{x}_{i/C}^2 + \dot{y}_{i/C}^2) + I_i \dot{\alpha}_i^2 + \sum_{j \in \mathcal{N}_i} (k_s(x_{i/j}^2 + y_{i/j}^2) + k_t \alpha_{i/j}^2) \right], \tag{43}$$

where the subscript i/j denotes the position or angle of appendage i relative to appendage j. The neighbor for the ith appendage $\mathcal{N}_i$ is the adjacent appendage that is closer to the hub, or the hub if the appendage attaches directly to the hub. Specifically $\mathcal{N}_i = i - 1$ for $i = (2, ..., N, N + 2, ..., 2N)$ and $\mathcal{N}_i = C$ for $i = 1, N + 1$.

Assume the spacecraft is intended to be nadir-pointing. Then the desired attitude for the spacecraft hub is such that frame $\mathcal{A}$ aligns with frame $\mathcal{P}$ and the desired angular velocity of the hub is the angular rate ω_O of the orbit. An artificial potential energy minimized by the hub's desired attitude and angular velocity is

$$U(\boldsymbol{\eta}_C) = \frac{1}{2} k_p(\gamma - \theta)^2 + \frac{1}{2} I_p(\dot{\gamma} - \omega_O)^2 \tag{44}$$

The candidate Lyapunov function is the summation of Eqs. (43) and (44), i.e.,

$$V(\boldsymbol{\eta}) = T(\boldsymbol{\eta}_p) + U(\boldsymbol{\eta}_C) \tag{45}$$

Consider a diagonal matrix describing the spring, mass, and inertia properties of the system, i.e.,

$$M = \text{diag}[k_p, I_{cs}, k_{s,1}, k_{s,1}, k_{t,1}, m_1, m_1, I_1, ..., k_{s,2N}, k_{s,2N}, k_{t,2N}, m_{2N}, m_{2N}, I_{2N}] \tag{46}$$

Consider also a graph Laplacian matrix that expresses the relative position and angle of adjacent appendages, i.e.,

$$\mathcal{L} = \text{diag}(\mathcal{L}_c, \mathcal{L}_1, \mathcal{L}_2, ..., \mathcal{L}_{N+1}, \mathcal{L}_{N+2}, ..., \mathcal{L}_{2N}) \tag{47}$$

where

$$\mathcal{L}_c = \mathcal{I}_2 \quad \mathcal{L}_{1,N+1} = \mathcal{I}_6 \quad \mathcal{L}_i = \begin{bmatrix} \text{diag}(-1, -1, -1, 0, 0, 0), & \mathcal{I}_6 \end{bmatrix} \tag{48}$$

$$\mathcal{L}_p = \text{diag}(\mathcal{L}_1, \mathcal{L}_2, ..., \mathcal{L}_{N+1}, \mathcal{L}_{N+2}, ..., \mathcal{L}_{2N}) \tag{49}$$

Let $\boldsymbol{\eta}_{c,d} = \begin{bmatrix} \gamma - \gamma_d & \omega - \omega_d \end{bmatrix}^T$ denote the orientation and angular velocity of the hub relative to the desired values. The state vector including these desired values is defined as $\boldsymbol{\eta}_d = \begin{bmatrix} \boldsymbol{\eta}_{c,d} & \boldsymbol{\eta}_p \end{bmatrix}^T$ The vector of relative states can then be taken using the graph Laplacian, i.e.,

$$\boldsymbol{\eta}_{rel} = \mathcal{L}\boldsymbol{\eta}_d \tag{50}$$

The Lyapunov function can then be written in matrix form

$$V(\boldsymbol{\eta}_{rel}) = \frac{1}{2}\boldsymbol{\eta}_{rel}^T M \boldsymbol{\eta}_{rel} \tag{51}$$

Differentiating with respect to time to yields

$$\dot{V}(\boldsymbol{\eta}_{rel}, \dot{\boldsymbol{\eta}}_{rel}) = \boldsymbol{\eta}_{rel}^T M \dot{\boldsymbol{\eta}}_{rel} \tag{52}$$

Because the linearized dynamics are exponentially stable, the stability characteristics of the nonlinear system in a neighborhood close to the origin can be approximated by the linearized dynamics [13]. $\dot{\boldsymbol{\eta}}_{rel} = A\boldsymbol{\eta}_{rel}$ is then substituted into $\dot{V}$ to yield

$$\dot{V}(\boldsymbol{\eta}_{rel}, \dot{\boldsymbol{\eta}}_{rel}) = \boldsymbol{\eta}_{rel}^T AM \dot{\boldsymbol{\eta}}_{rel} \tag{53}$$

For convenience of analyzing the Lyapunov function derivative, the output is collected into two terms relating to the energy of the hub, denoted $\dot{V}_C$, and the appendages, denoted $\dot{V}_p$, such that $\dot{V} = \dot{V}_C + \dot{V}_p$. The splitting is carried out as follows

$$\dot{V} = \begin{bmatrix} (\mathcal{L}_c \boldsymbol{\eta}_{c,d})^T \\ (\mathcal{L}_p \boldsymbol{\eta}_p)^T \end{bmatrix} \begin{bmatrix} MA_C \\ MA_i \end{bmatrix} \begin{bmatrix} \boldsymbol{\eta}_{rel} \\ \boldsymbol{\eta}_{rel} \end{bmatrix} + \begin{bmatrix} (\mathcal{L}_c \boldsymbol{\eta}_{c,d})^T \\ (\mathcal{L}_p \boldsymbol{\eta}_p)^T \end{bmatrix} \begin{bmatrix} B_C \\ B_i \end{bmatrix} \begin{bmatrix} u_{rw} \\ u_1 \\ \vdots \\ u_{2N} \end{bmatrix} = \begin{bmatrix} \dot{V}_C \\ \dot{V}_p \end{bmatrix}, \tag{54}$$

where A_C and B_C are the first two rows of the the Jacobian matrix A, and A_i and B_i consist of the remaining rows of matrices A and B.

The expression for V_p can be expanded to

$$\dot{V}_p = \boldsymbol{\eta}_p^T M A_i \boldsymbol{\eta} + \boldsymbol{\eta}_p^T M B_i \mathbf{u}_i. \tag{55}$$

The first term in the expression may be expressed as $\boldsymbol{\eta}_p^T M A_i \boldsymbol{\eta}_p$ where A_i excludes the first two columns of $A_{i,c}$ to make it a square matrix. This truncation does not change the value of $\dot{V}_p$ because the state variables of the appendages are expressed in the hub's reference frame and thus do not depend on the state of the hub. With the exclusion of the dynamics of the hub, the two zero eigenvalues are also excluded, thus A_i is Hurwitz. Because M is positive definite, the product MA_i is also Hurwitz. Consequently,

$$\boldsymbol{\eta}_p^T M A_i \boldsymbol{\eta} < 0. \tag{56}$$

Assuming that the spacecraft is near the equilibrium, then the translational velocities of each appendage relative to the hub are small. Under this assumption, expressed in Eq. (41), the expansion of the second term is

$$\boldsymbol{\eta}_p^T B_i \mathbf{u}_i = E \sum_{i=1}^{2N} \dot{\alpha}_i u_i + \text{H.O.T} \tag{57}$$

This expression suggests that a control law for each torque rod of

$$m_i = -\text{dbd}(\dot{\alpha}_i) K_{tr} \tag{58}$$

will both guarantee that $\boldsymbol{\eta}_p^T M B_i \mathbf{u}_i \leq 0$ and will minimize $\dot{V}_p$ subject to the the control constraints of the torque rods. Because each term is negative definite, $\dot{V}_p < 0$.

V_C is now considered. Expanding the expression

$$\dot{V}_C = \boldsymbol{\eta}_C^T M A_C \boldsymbol{\eta} + \boldsymbol{\eta}_C^T M B_C u_{rw}, \tag{59}$$

yields

$$\dot{V}_C = (\dot{\gamma} - \omega_O)(k_p(\gamma - \theta) + \beta_C(\dot{\alpha}_1 + \dot{\alpha}_{N+1}) + \beta_k(\alpha_1 + \alpha_{N+1}) + u_{rw}) - u_{rw}\frac{I_p}{I_C}\sum_{i=1}^{2N}\dot{\alpha}_i, \tag{60}$$

where constants β_C and β_k are defined as

$$\beta_k = k_t - \frac{Lk_s s}{4} \tag{61}$$

$$\beta_C = c_t - \frac{Lc_s s}{4} \tag{62}$$

The following control law is proposed:

$$u_{rw} = -\beta_C(\dot{\alpha}_1 + \dot{\alpha}_{N+1}) - \beta_k(\alpha_1 + \alpha_{N+1}) - k_p(\gamma - \theta) - k_L(\dot{\gamma} - \omega_O) \tag{63}$$

Under the assumptions made in Equations (39) to (42),

$$u_{rw}\frac{I_p}{I_C}\sum_{i=1}^{2N}\dot{\alpha}_i \approx 0. \tag{64}$$

Substituting the proposed control law into $\dot{V}_C$ then yields

$$\dot{V}_C = -k_L(\dot{\gamma} - \omega_O)^2, \tag{65}$$

which means that $\dot{V}_C \leq 0$ under the proposed control law. Consider the set $S = \{\boldsymbol{\eta}_d | \dot{V}_C = 0\} = \{\boldsymbol{\eta}_d | \dot{\gamma} = \omega_O\}$. The proposed controller is such that actuation will be applied when the state is not in the equilibrium state, therefore any trajectory where $\dot{\gamma} = \omega_O$ except the equilibrium state is not contained in S. Establihsing convergence via the invariance principle [13] is the subject of ongoing work.

From a practical standpoint, the control law resulting from Lyapunov analysis is favorable for implementation. The torque rod control law acts in the opposite direction of the angular velocity of the appendage relative to the hub. It is also computationally simple and easily implementable using angular velocity measured with gyros. The control law for the reaction wheel contains proportional and derivative control terms with tuneable gains, and also terms that become relevant if the appendages directly affixed to the hub are not flat.

V. Simulation Results

Numerical simulations illustrate the performance of the closed-loop system. To better understand controller behavior and performance, several controllers were simulated and compared. In addition to the proposed Lyapunov-based controller, an LQR with the saturation and deadband functions shown in Section III.C applied to the control signal was also simulated. To better understand the effect of the torque rods on system performance the Lyapunov-based controller without β_k, β_c, and the torque rod inputs was also tested leaving a proportional-derivative controller for the reaction wheel was also performed.

A. Idealized Model

The first simulation assumes an idealized scenario where there are no disturbance forces or moments. Assume that the torque generated by the torque rods is not subject to varying magnitudes due to the different angles of incidence with the magnetic field lines of the Earth, and instead that the maximum control authority is available to the torque rods at all times, i.e., $\tau_{\text{tr}} = 2H_e(\frac{R}{\rho})^3 u_i$. The goal of the controllers is to track a reference pointing angle $\theta(t) = w_0 t$, which is the angular position of a 400km altitude circular orbit. The initial state of the spacecraft is at equilibrium with $\gamma = 15°$, and the initial angular velocity is ω_O. The parameters for the simulation are shown in Table 1. The dbd function from Eq. (25) is used instead of the sgn function, because as $\lambda \to 0$ the dbd function becomes the sgn function, and the dbd function is preferable for implementation as it reduces chatter.

parameter	N	m_C	m_i	I_C	I_i	L_i	L_C	k_s	c_s	k_t	c_t	w_0	K_{rw}	K_{tr}
value	12	100	1	50	0.1	1	2	100	0.1	10	0.1	1.2×10^{-3}	0.01	1×10^{-4}
unit		kg	kg	kgm^2	kgm^2	m	m	$\frac{\text{N}}{\text{m}}$	$\frac{\text{Ns}}{\text{m}}$	$\frac{\text{Nm}}{\text{rad}}$	$\frac{\text{Nms}}{\text{rad}}$	$\frac{\text{rad}}{\text{s}}$	Nm	Nm

Table 1 Simulation Parameters

The two primary performance metrics used to measure the overall flatness of the system are the mean squared angular error and the distance between the two end appendages (N and $2N$) in the $\hat{\mathbf{a}}_2$ direction, i.e., $|y_{N/c} - y_{2N/c}|$. These metrics are shown in Fig. 4.The actuation effort for the reaction wheel and the torque rod on the appendage $i = 1$ are shown in Fig. 5. Finally, the error in attitude pointing angle is also displayed in Fig. 6.

angle error.png

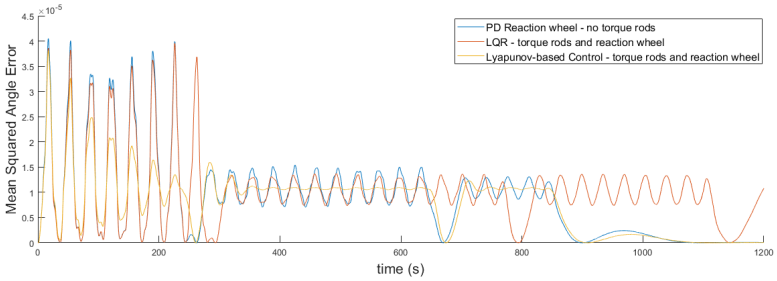

(a) Mean squared angle error

e2e flatness.png

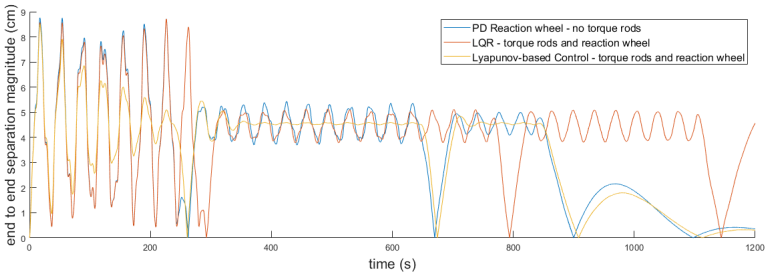

(b) End-to-end separation

Fig. 4 Comparison of the control performance of PD, LQR, and Lyapunov-based controllers over a 1400 second simulation. The mean squared angle error is shown in (a) and the difference in vertical displacement between the two end appendages is shown in (b). The Lyapunov-based controller damps oscillations from the system more quickly than the other two controllers.

rw input.png

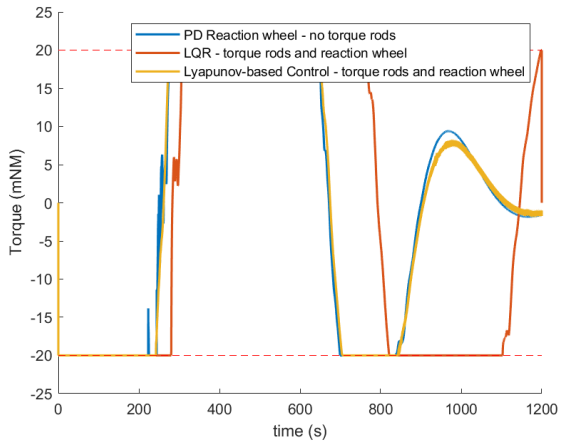

(a) Reaction Wheel Input

tr input.png

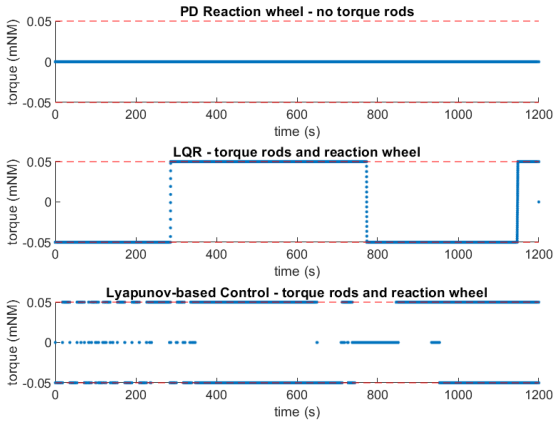

(b) Torque Rod Input

Fig. 5 Comparison of the control performance of PD, LQR, and Lyapunov-based controllers over a 1400 second simulation. The reaction wheel control histories is shown in (a) and the torque rod control history for appendage $i = 1$ is shown in (b). The LQR controller attempts to use the torque rods to assist in the attitude control, as the control inputs mirror each other, whereas the Lypaunov controller mirrors the oscillations shown in the performance metrics because it is used to damp out the oscillations in the appendages.

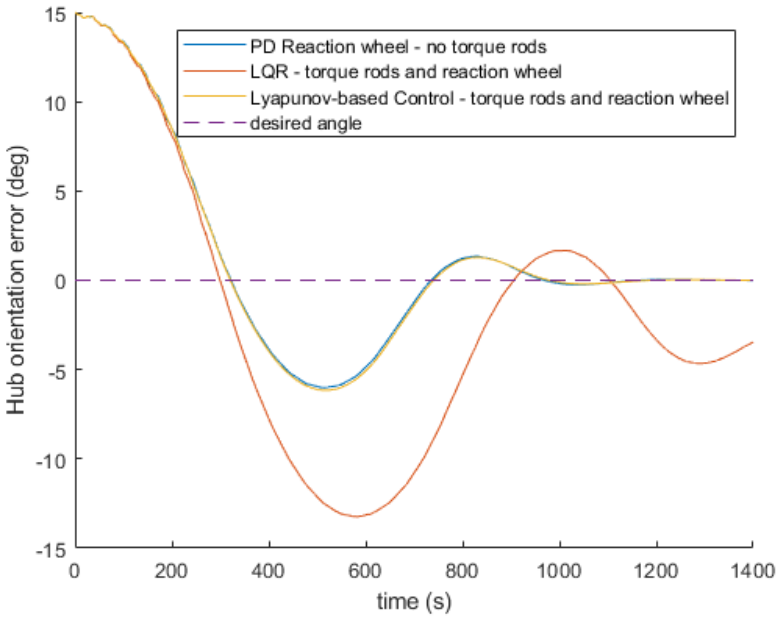

gamma.png

Fig. 6 Comparison of the control performance of PD, LQR, and Lyapunov-based controllers over a 1400 second simulation.

Simulations show that the Lyapunov-based controller performs better than either of the other two controllers. Compared with the PD reaction wheel and no torque rods, the high frequency oscillations induced by the control input damps out much more quickly. After about 400 seconds, the oscillations are mostly suppressed, and the angular error that remained is constant as a result of the constant torque induced by the reaction wheel. Slight oscillations are introduced again when the reaction wheel changed the direction of applied torque, but those are again quickly damped

out. The LQR controller performs slightly better than the controller absent torque rods with respect to flatness, but the attitude pointing performance was much worse, likely a result of the enforced controller saturation.

B. Orbital Model

A second simulation was performed where the following orbital effects were included: orbital dynamics of the spacecraft, the disturbance resulting from gravity gradient torque modeled in Eq. (26), and the time-varying effects of the orientation of the torque rods relative to Earth's magnetic field in Eq. (25). The same initial conditions are used as in the first simulation; assume that the spacecraft is in a 400km altitude polar orbit, where, at $t = 0$, the spacecraft is at a colatitude of 0. The same plots are shown as before, but with the inclusion of the maximum torque available to the $i = 1$ torque rod for the duration of the simulation.

angle error.png

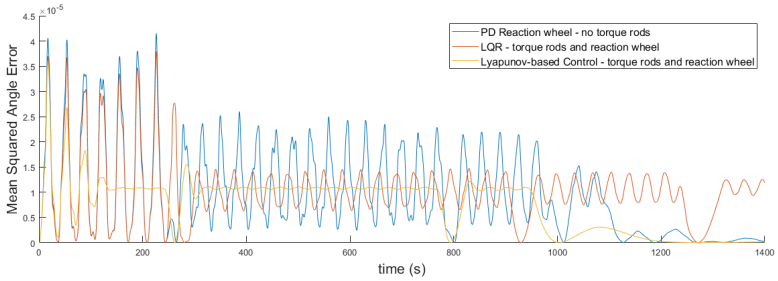

(a) Mean squared angle error

e2e flatness.png

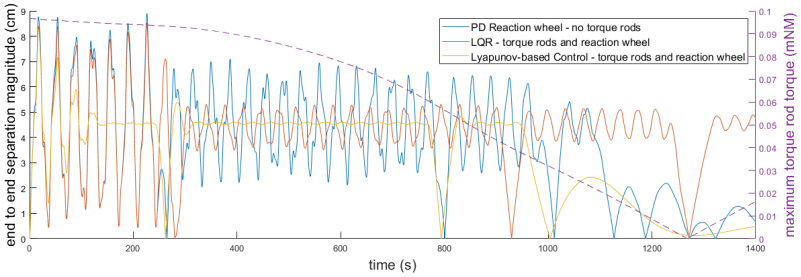

(b) End-to-end separation

Fig. 7 Comparison of the control performance of PD, LQR, and Lyapunov-based controllers over a 1400 second on-orbit simulation. The mean squared angle error is shown in (a) and the difference in vertical displacement between the two end appendages is shown in (b). The Lyapunov-based controller damps oscillations from the system more quickly than the other two controllers.

rw input.png

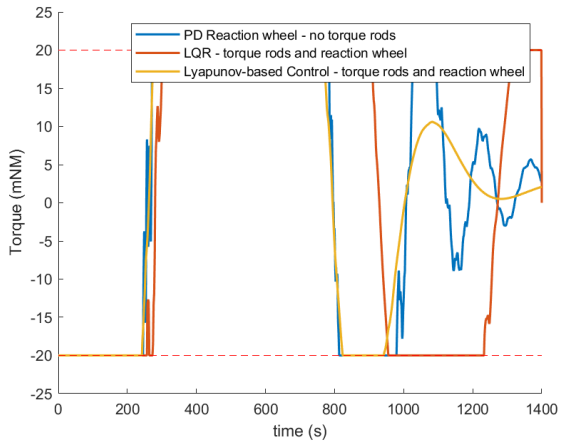

(a) Reaction Wheel Input

tr input.png

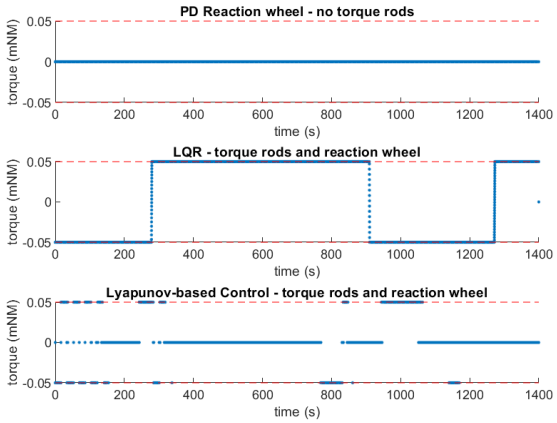

(b) Torque Rod Input

Fig. 8 Comparison of the control performance of PD, LQR, and Lyapunov-based controllers over a 1400 second on-orbit simulation. The mean squared angle error is shown in (a) and the difference in $\hat{a}_2$ displacement between the two end appendages is shown in (b). The Lyapunov-based controller damps oscillations from the system more quickly than the other two controllers.

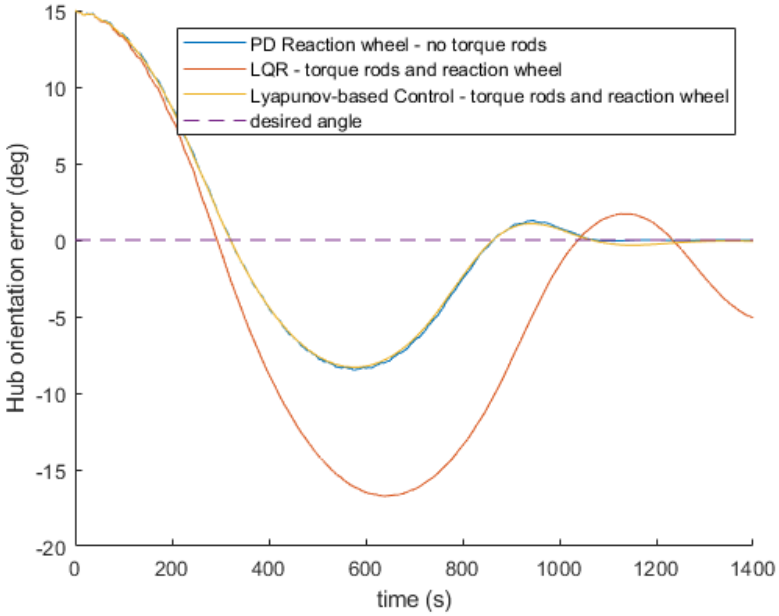

gamma.png

Fig. 9 Comparison of the control performance of PD, LQR, and Lyapunov-based controllers over a 1400 second on-orbit simulation.

The simulation with disturbances and on-orbit effects shows that the performance improvement of the proposed controller is even larger than in the idealized case. The addition of the disturbances causes the unforced torque rod case to perform much worse, increasing the magnitude and time to decay of the induced oscillations. The simulation also demonstrates that the proposed controller performs as expected with unknown disturbances and with the control saturation varying over time.

VI. Conclusion

This paper derives a feedback control law for a spacecraft model consisting of a central hub and multiple flexibly connected appendages on either side of this hub. This model could represent either the flexibility of a large single appendage or the behavior of a deployable space structure after it had been deployed. To control the shape and attitude of this model, actuation consisting of a reaction wheel on the hub and magnetic torque rods on each of the appendages is proposed. Springs to model internal forces and moments, external disturbances, and actuator constraints are considered in modeling the dynamics of the system. The nonlinearities in the model suggest a Lyapunov-based approach to the control design. By performing Lyapunov analysis on the system dynamics, feedback control laws for the reaction wheel and each torque rod are obtained. Numerical simulations show that the proposed controller removes vibrations from the system more quickly than both a system without torque rods, and a system with torque rods but with a different control law.

Future work includes the extension of this model to a full three-dimensional model where the hinges are able to bend in two directions instead of one and where there are out of plane appendages are considered as well. With a higher dimensional model, similar analyses will be performed to investigate possible controllers for the higher dimensional system.

References

[1] Nadafi, R., Kabganian, M., Kamali, A., and Hossein Nejad, M., "Super-twisting sliding mode control design based on Lyapunov criteria for attitude tracking control and vibration suppression of a flexible spacecraft," *Measurement and Control*, Vol. 52, No. 7-8, 2019, p. 814–831. https://doi.org/10.1177/0020294019847696.

[2] Yan, R., and Wu, Z., "Attitude Stabilization of flexible spacecrafts via extended disturbance observer based controller," *Acta Astronautica*, Vol. 133, 2017, p. 73–80. https://doi.org/10.1016/j.actaastro.2017.01.004.

[3] Ji, N., and Liu, J., "Distributed vibration control for flexible spacecraft with distributed disturbance and actuator fault," *Journal of Sound and Vibration*, Vol. 475, 2020, p. 115274. https://doi.org/10.1016/j.jsv.2020.115274.

[4] Zhong, C., Chen, Z., and Guo, Y., "Attitude control for flexible spacecraft with disturbance rejection," *IEEE Transactions on Aerospace and Electronic Systems*, Vol. 53, No. 1, 2017, p. 101–110. https://doi.org/10.1109/taes.2017.2649259.

[5] Fracchia, G., Biggs, J. D., and Ceriotti, M., "Analytical low-jerk reorientation maneuvers for multi-body spacecraft structures," *Acta Astronautica*, Vol. 178, 2021, p. 1–14. https://doi.org/10.1016/j.actaastro.2020.08.020.

[6] Cao, X., Yue, C., and Liu, M., "Flexible satellite attitude maneuver via constrained torque distribution and active vibration suppression," *Aerospace Science and Technology*, Vol. 67, 2017, p. 387–397. https://doi.org/10.1016/j.ast.2017.04.014.

[7] Sun, J., Li, S., Huang, J., and Zhu, D., "Robust coordinated control for large flexible spacecraft based on consensus theory," *Journal of the Franklin Institute*, Vol. 357, No. 9, 2020, p. 5359–5379. https://doi.org/10.1016/j.jfranklin.2020.02.049.

[8] Fulton, J., and Schaub, H., "Deployment Dynamics Analysis of an origami-folded spacecraft structure with elastic hinges," *Journal of Spacecraft and Rockets*, Vol. 59, No. 2, 2022, p. 401–420. https://doi.org/10.2514/1.a34938.

[9] Zhang, Y., and Guan, X., "Active damping control of flexible appendages for spacecraft," *Aerospace Science and Technology*, Vol. 75, 2018, p. 237–244. https://doi.org/10.1016/j.ast.2017.12.027.

[10] Hu, Q., Jia, Y., and Xu, S., "Dynamics and vibration suppression of space structures with control moment gyroscopes," *Acta Astronautica*, Vol. 96, 2014, p. 232–245. https://doi.org/10.1016/j.actaastro.2013.11.032.

[11] Feng, X., Jia, Y., and Xu, S., "Dynamics of flexible multibody systems with variable-speed control moment gyroscopes," *Aerospace Science and Technology*, Vol. 79, 2018, p. 554–569. https://doi.org/10.1016/j.ast.2018.06.004.

[12] Wie, B., *Space Vehicle Dynamics and control*, American Institute of Aeoronautics and Astronautics, Inc., 2008.

[13] Khalil, H. K., *Nonlinear systems*, Prentice Hall, 2002.

VII. Appendix

A. Internal Forces and Moments

The force terms for each spacecraft component are shown. For an appendage that has two appendages on either side of it and is on the right side of the hub, $i \in [2, N-1]$, the forces and moments are as follows:

$$X_{i,i+1} = k_s \left(x_{i+1/C} - x_{i/C} - \frac{L_{i+1}}{2}\cos\alpha_{i+1} - \frac{L_i}{2}\cos\alpha_i \right) + c_s \left(\dot{x}_{i+1/C} - \dot{x}_{i/C} + \frac{L_{i+1}}{2}\dot{\alpha}_{i+1}\sin\alpha_{i+1} + \frac{L_i}{2}\dot{\alpha}_i \sin\alpha_i \right)$$

$$X_{i,i-1} = -k_s \left(x_{i/C} - x_{i-1/C} - \frac{L_i}{2}\cos\alpha_i - \frac{L_{i-1}}{2}\cos\alpha_{i-1} \right) + c_s \left(\dot{x}_{i/C} - \dot{x}_{i-1/C} + \frac{L_i}{2}\dot{\alpha}_i\sin\alpha_i + \frac{L_{i-1}}{2}\dot{\alpha}_{i-1}\sin\alpha_{i-1} \right)$$

$$Y_{i,i+1} = k_s \left(y_{i+1/C} - y_{i/C} - \frac{L_{i+1}}{2}\sin\alpha_{i+1} - \frac{L_i}{2}\sin\alpha_i \right) + c_s \left(\dot{y}_{i+1/C} - \dot{y}_{i/C} + \frac{L_{i+1}}{2}\dot{\alpha}_{i+1}\cos\alpha_{i+1} + \frac{L_i}{2}\dot{\alpha}_i\cos\alpha_i \right)$$

$$Y_{i,i-1} = -k_s \left(y_{i/C} - y_{i-1/C} - \frac{L_i}{2}\sin\alpha_i - \frac{L_{i-1}}{2}\sin\alpha_{i-1} \right) + c_s \left(\dot{y}_{i/C} - \dot{y}_{i-1/C} + \frac{L_i}{2}\dot{\alpha}_i\cos\alpha_i + \frac{L_{i-1}}{2}\dot{\alpha}_{i-1}\cos\alpha_{i-1} \right)$$

$$T_{i,i+1} = \frac{L_i}{2}\cos\alpha_i Y_{i,i+1} - \frac{L_i}{2}\sin\alpha_i X_{i,i+1}$$

$$T_{i,i-1} = -\frac{L_i}{2}\cos\alpha_i X_{i,i-1} + \frac{L_i}{2}\sin\alpha_i Y_{i,i-1}$$

$$M_{i,i+1} = k_t(\alpha_{i+1} - \alpha_i) + c_t(\dot{\alpha}_{i+1} - \dot{\alpha}_i)$$

$$M_{i,i-1} = -k_t(\alpha_i - \alpha_{i-1}) - c_t(\dot{\alpha}_i - \dot{\alpha}_{i-1})$$

For appendages on the left that have a appendage on either side, $i \in [N+2, 2N-1]$, the forces and moments are the negation of what is shown above, because the indexing goes in the opposite direction.

For the appendage where $i = 1$ the forces and moments are as follows.

$$X_{1,2} = k_s \left(x_{2/C} - x_{1/C} - \frac{L_2}{2}\cos\alpha_2 - \frac{L_1}{2}\cos\alpha_1 \right) + c_s \left(\dot{x}_{2/C} - \dot{x}_{1/C} + \frac{L_2}{2}\dot{\alpha}_2\sin\alpha_2 + \frac{L_1}{2}\dot{\alpha}_1\sin\alpha_1 \right)$$

$$\begin{aligned} X_{1,C} &= -k_s \left(x_{1/C} - x_{c/c} - \frac{L_1}{2}\cos\alpha_1 - \frac{L_C}{2}\cos\gamma \right) + c_s \left(\dot{x}_{1/C} - \dot{x}_{c/c} + \frac{L_1}{2}\dot{\alpha}_1\sin\alpha_1 + \frac{L_C}{2}\dot{\alpha}_c\sin\gamma \right) \\ &= -k_s \left(x_{1/C} - \frac{L_1}{2}\cos\alpha_1 - \frac{L_C}{2} \right) + c_s \left(\dot{x}_{1/C} + \frac{L_1}{2}\dot{\alpha}_1\sin\alpha_1 \right) \end{aligned}$$

$$Y_{1,2} = k_s \left(y_{2/C} - y_{1/C} - \frac{L_2}{2}\sin\alpha_2 - \frac{L_1}{2}\sin\alpha_1 \right) + c_s \left(\dot{y}_{2/C} - \dot{y}_{1/C} + \frac{L_2}{2}\dot{\alpha}_2\cos\alpha_2 + \frac{L_1}{2}\dot{\alpha}_1\cos\alpha_1 \right)$$

$$\begin{aligned} Y_{1,C} &= -k_s \left(y_{1/C} - y_{c/c} - \frac{L_1}{2}\sin\alpha_1 - \frac{L_C}{2}\sin\gamma \right) + c_s \left(\dot{y}_{1/C} - \dot{y}_{c/c} + \frac{L_1}{2}\dot{\alpha}_1\cos\alpha_1 + \frac{L_C}{2}\dot{\alpha}_c\cos\gamma \right) \\ &= -k_s \left(y_{1/C} - \frac{L_1}{2}\sin\alpha_1 \right) + c_s \left(\dot{y}_{1/C} + \frac{L_1}{2}\dot{\alpha}_1\cos\alpha_1 \right) \end{aligned}$$

$$T_{1,2} = \frac{L_1}{2}\cos\alpha_1 Y_{1,2} - \frac{L_1}{2}\sin\alpha_1 X_{1,2}$$

$$T_{1,C} = -\frac{L_1}{2}\cos\alpha_1 X_{1,C} + \frac{L_1}{2}\sin\alpha_1 Y_{1,C}$$

$$M_{1,2} = k_t(\alpha_2 - \alpha_1) + c_t(\dot{\alpha}_2 - \dot{\alpha}_1)$$

$$\begin{aligned} M_{1,C} &= -k_t(\alpha_1 - \gamma) - c_t(\dot{\alpha}_1 - \dot{\alpha}_C) \\ &= -k_t(\alpha_1) - c_t(\dot{\alpha}_1) \end{aligned}$$

For the appendage $i = N + 1$, which is the appendage directly to the left of the hub

$$X_{N+1,C} = k_s\left(-x_{N+1/C} - \frac{L_C}{2} - \frac{L_{N+1}}{2}\cos\alpha_{N+1}\right) + c_s\left(-\dot{x}_{N+1/C} + \frac{L_{N+1}}{2}\dot{\alpha}_{N+1}\sin\alpha_{N+1}\right)$$

$$\begin{aligned} X_{N+1,N+2} = &- k_s\left(x_{N+1/C} - x_{N+2/C} - \frac{L_{N+1}}{2}\cos\alpha_{N+1} - \frac{L_{N+2}}{2}\cos\alpha_{N+2}\right) \\ &+ c_s\left(\dot{x}_{N+1/C} - \dot{x}_{N+2/C} + \frac{L_{N+1}}{2}\dot{\alpha}_{N+1}\sin\alpha_{N+1} + \frac{L_{N+2}}{2}\dot{\alpha}_{N+2}\sin\alpha_{N+2}\right) \end{aligned}$$

$$Y_{N+1,C} = k_s\left(-y_{N+1/C} - \frac{L_{N+1}}{2}\sin\alpha_{N+1}\right) + c_s\left(-\dot{y}_{N+1/C} + \frac{L_{N+1}}{2}\dot{\alpha}_{N+1}\cos\alpha_{N+1}\right)$$

$$\begin{aligned} Y_{N+1,N+2} = &- k_s\left(y_{N+1/C} - y_{N+2/C} - \frac{L_{N+1}}{2}\sin\alpha_{N+1} - \frac{L_{N+2}}{2}\sin\alpha_{N+2}\right) \\ &+ c_s\left(\dot{y}_{N+1/C} - \dot{y}_{N+2/C} + \frac{L_{N+1}}{2}\dot{\alpha}_{N+1}\cos\alpha_{N+1} + \frac{L_{N+2}}{2}\dot{\alpha}_{N+2}\cos\alpha_{N+2}\right) \end{aligned}$$

$$T_{N+1,C} = \frac{L_{N+1}}{2}\cos\alpha_{N+1} Y_{N+1,C} - \frac{L_{N+1}}{2}\sin\alpha_{N+1} X_{N+1,C}$$

$$T_{N+1,N+2} = -\frac{L_{N+1}}{2}\cos\alpha_{N+1} X_{N+1,N+2} + \frac{L_{N+1}}{2}\sin\alpha_{N+1} Y_{N+1,N+2}$$

$$M_{N+1,C} = k_t(-\alpha_{N+1}) + c_t(-\dot{\alpha}_{N+1})$$

$$M_{N+1,N+2} = -k_t(\alpha_{N+1} - \alpha_{N+2}) - c_t(\dot{\alpha}_{N+1} - \dot{\alpha}_{N+2})$$

For the case of the end appendage, $i = N$, the same equations as the middle appendages between $i = 1$, and $i = N$ are used, except $X_{i,i+1}, Y_{i,i+1}, T_{i,i+1}, M_{i,i+1}$ are all zero, because there is only one adjacent appendage. Similarly, for the other end appendage, $i = 2N$, the equations for $i \in [N + 2, 2N - 1]$ can be used, where $X_{i,i+1}, Y_{i,i+1}, T_{i,i+1}, M_{i,i+1}$ are also all zero. The forces and moments acting on the hub are equal and opposite to those acting on the appendages attached to the hub, i.e.,

$$\begin{aligned} X_{C,1} &= -X_{1,C} \\ X_{C,N+1} &= -X_{N+1,C} \\ Y_{C,1} &= -Y_{1,C} \\ Y_{C,N+1} &= -Y_{N+1,C} \\ T_{C,1} &= \tfrac{L_c}{2} Y_{C,1} \\ T_{C,N+1} &= -\tfrac{L_c}{2} Y_{C,N+1} \\ M_{C,1} &= -M_{1,C} \\ M_{C,N+1} &= -M_{N+1,C} \end{aligned}$$

The total forces and moments are

$$
\begin{aligned}
X_i &= X_{i,i+1} + X_{i,i-1} \\
Y_i &= Y_{i,i+1} + Y_{i,i-1} \\
T_i &= T_{i,i+1} + T_{i,i-1} \\
M_i &= M_{i,i+1} + M_{i,i-1}
\end{aligned}
$$

$$
\begin{aligned}
X_c &= X_{C,1} + X_{C,N} \\
Y_c &= Y_{C,1} + Y_{C,N} \\
T_c &= T_{C,1} + T_{C,N} \\
M_c &= M_{C,1} + M_{C,N}
\end{aligned}
$$